J. Fluid Mech. (1993), *vol.* 253, *pp.* 663–680

Two-dimensional oscillatory convection in a gravitationally modulated fluid layer

By R. CLEVER[1], G. SCHUBERT[1] AND F. H. BUSSE[2]

[1] Institute of Geophysics and Planetary Physics, University of California, Los Angeles, CA 90024, USA

[2] Physikalisches Institut, Universität Bayreuth, Postfach 101251, D8580 Bayreuth, Germany

(Received 16 July 1992 and in revised form 16 February 1993)

A Galerkin method is used to study the two-dimensional modes of oscillatory convection in a gravitationally modulated fluid layer with rigid, isothermal boundaries heated either from below or from above. Nonlinear solutions are obtained for dimensionless frequencies ω (frequency is made non-dimensional with the timescale d^2/κ where d is the depth of the fluid layer and κ is the thermal diffusivity) in the range 100–3000, dimensionless accelerations ϵ (ϵg is the amplitude of the externally imposed oscillatory vertical acceleration and g is the constant vertical acceleration of gravity) in the range of 1–10^4, and Prandtl numbers P in the range 0.71 (air) to 7 (water). The problem of convective onset is explored for a broader range of parameters than heretofore considered, including Prandtl numbers between 0.71 and 50. Both synchronous and subharmonic modes of convection are identified and it is found that finite-amplitude synchronous convection can be unstable to subharmonic modes.

1. Introduction

Studies of thermal convection in externally modulated fluid layers have mainly dealt with the weakly nonlinear motions near the onset of convection. These include the early work of Venezian (1969), Gresho & Sani (1970), Rosenblat & Herbert (1970) and Rosenblat & Tanaka (1971) (see also the review by Davis 1976). The paper by Burde (1970) and other Russian works that are not well known in the Western literature are also relevant, and these have been reviewed in Gershuni & Zhukovitskii (1976). More recently this body of work has been extended by Roppo, Davis & Rosenblat (1984), Ahlers, Hohenberg & Lücke (1985*a*) and Hohenberg & Swift (1987). A number of experiments have also been performed on the influence of modulation on the onset of convection (Finucane & Kelly 1976; Ahlers, Hohenberg & Lücke 1985*b*; Niemela & Donnelly 1987; see also the recent review by Donnelly 1990). Reasonable agreement between theoretical predictions and experimental measurements has been obtained.

As shown by Gresho & Sani (1970), the Rayleigh number for onset of synchronous convection increases with increasing frequency of modulation for a layer oscillating with constant vertical displacement amplitude until a certain frequency is reached at which the onset is in the form of subharmonic motions. Synchronous and subharmonic modes of convection also occur at finite amplitude, as demonstrated by Gresho & Sani (1970) and more recently by Biringen & Peltier (1990). However, relatively little is known of the quantitative effects of modulation on the onset of convection over a wide range of modulation frequencies and amplitudes and Prandtl numbers, and even less is known about the heat transfer properties and stabilities of the nonlinear modes of convection. Because the oscillations tend to affect the phase relationships between the

temperature and velocity fields, the heat transport properties may be affected by the modulation even more than the critical Rayleigh number for onset of convection. These nonlinear effects are of basic interest, but they also have important applications, e.g. crystallization from a melt in the low-gravity environment of orbiting space stations.

The research presented in this paper addresses both the onset of convection and the finite-amplitude motions of a bottom or top heated fluid layer under the influence of a gravitational modulation, i.e. an externally imposed oscillatory acceleration in the same direction as the steady acceleration of gravity. Prandtl numbers in the range 0.71–50, dimensionless frequencies in the range 30–6000 and non-dimensional amplitudes of the imposed oscillatory acceleration up to several thousand are considered. The motions are either synchronous for small values of the frequency or subharmonic for large frequency values. The stability of the solutions to disturbances confined to two spatial dimensions is investigated.

2. Mathematical formulation

2.1. *Basic equations*

We consider a vertically oscillating horizontal Boussinesq fluid layer of thickness d which is heated from either above or below. The dimensionless equations of continuity, motion, and temperature are:

$$\nabla \cdot \boldsymbol{v} = 0, \tag{2.1}$$

$$\nabla^2 \boldsymbol{v} + \boldsymbol{k}(1 + \epsilon \cos \omega t) - \nabla \Gamma = \frac{1}{P}\left(\boldsymbol{v} \cdot \nabla \boldsymbol{v} + \frac{\partial \boldsymbol{v}}{\partial t}\right), \tag{2.2}$$

$$\nabla^2 \theta + R\boldsymbol{k} \cdot \boldsymbol{v} = \boldsymbol{v} \cdot \nabla \theta + \frac{\partial \theta}{\partial t}. \tag{2.3}$$

In (2.1)–(2.3) we use d as a lengthscale, d^2/κ as a timescale, and $\Delta T/R$ as a temperature scale, where ΔT is the temperature difference between the upper and lower boundaries defined to be positive for bottom heating, κ is the thermal diffusivity, and R is the Rayleigh number defined by

$$R = \frac{\bar{\alpha} g \Delta T d^3}{\kappa \nu}, \tag{2.4}$$

with $\bar{\alpha}$ the thermal expansivity, g the steady acceleration due to gravity (gravity points vertically downward in the direction opposite to the unit vector $\boldsymbol{k}$ in the upward z-direction), and ν the kinematic viscosity. The temperature difference ΔT and R are negative for heating from above. The non-dimensional convective velocity is $\boldsymbol{v}$, the dimensionless pressure is Γ, and θ is the dimensionless deviation in temperature from the steady conductive state with a linear temperature *vs.* height profile. The Prandtl number P is ν/κ. The imposed vertical acceleration has non-dimensional frequency ω and dimensionless amplitude ϵ (scaled by g). The dimensionless horizontal coordinate is x and the origin of the coordinate system is at the midplane of the layer. The dependence of convection on the physical conditions of the problem is expressed by the four dimensionless parameters R, P, ω and ϵ and the boundary conditions at the top and bottom rigid, isothermal surfaces.

In the Boussinesq approximation, and for two-dimensional motions, the equation of continuity (2.1) can be eliminated from the problem by introducing the following general representation of the solenoidal velocity field:

$$\boldsymbol{v} = \delta \phi \tag{2.5}$$

where the operator $\boldsymbol{\delta}$ is defined by

$$\boldsymbol{\delta}\phi = \boldsymbol{\nabla} \times (\boldsymbol{\nabla} \times \boldsymbol{k}\phi). \tag{2.6}$$

Upon substitution of (2.5) and (2.6) into (2.2) and (2.3) we obtain the following equations for the scalar variables ϕ and θ:

$$\partial_x(\nabla^4\phi - (1+\epsilon\cos\omega t)\,\theta)$$

$$= \frac{1}{P}\left\{\partial^2_{xz}\phi\partial^4_{xxzz}\phi - \partial^2_{xx}\phi\partial^4_{xzzz}\phi + \partial^2_{xz}\phi\partial^4_{xxxx}\phi - \partial^2_{xx}\phi\partial^4_{xxxz}\phi + \frac{\partial}{\partial t}(\partial_x\nabla^2\phi)\right\}, \tag{2.7}$$

$$\nabla^2\theta - R\partial^2_{xx}\phi = \partial^2_{xz}\phi\partial_x\theta - \partial^2_{xx}\phi\partial_z\theta + \frac{\partial\theta}{\partial t}. \tag{2.8}$$

The boundary conditions are given by

$$\phi = \partial_z\phi = \theta = 0 \quad \text{at} \quad z = \pm\tfrac{1}{2}. \tag{2.9}$$

2.2. *Finite-amplitude convection*

Because of the externally imposed time dependence represented by $(1+\epsilon\cos\omega t)$ in (2.2), the Galerkin solution must be sought in the form

$$\phi = \sum_{\substack{\beta\lambda\nu \\ (\lambda+\nu)\text{even}}} (\hat{a}_{\beta\lambda\nu}\cos\beta\omega t + \check{a}_{\beta\lambda\nu}\sin\beta\omega t)(\cos\lambda\alpha x)\,g_\nu(z) \equiv \sum_{\beta\lambda\nu} \hat{a}_{\beta\lambda\nu}\hat{\phi}_{\beta\lambda\nu} + \check{a}_{\beta\lambda\nu}\check{\phi}_{\beta\lambda\nu}, \tag{2.10}$$

$$\theta = \sum_{\substack{\beta\lambda\nu \\ (\lambda+\nu)\text{even}}} (\hat{b}_{\beta\lambda\nu}\cos\beta\omega t + \check{b}_{\beta\lambda\nu}\sin\beta\omega t)(\cos\lambda\alpha x)f_\nu(z) \equiv \sum \hat{b}_{\beta\lambda\nu}\hat{\theta}_{\beta\lambda\nu} + \check{b}_{\beta\lambda\nu}\check{\theta}_{\beta\lambda\nu}. \tag{2.11}$$

The functions

$$g_\nu(z) = \begin{cases} \dfrac{\sinh(\hat{\gamma}_{\frac{1}{2}\nu}z)}{\sinh(\frac{1}{2}\hat{\gamma}_{\frac{1}{2}\nu})} - \dfrac{\sin(\hat{\gamma}_{\frac{1}{2}\nu}z)}{\sin(\frac{1}{2}\hat{\gamma}_{\frac{1}{2}\nu})} & \text{for } \nu \text{ even} \\ \dfrac{\cosh(\check{\gamma}_{\frac{1}{2}(\nu+1)}z)}{\cosh(\frac{1}{2}\check{\gamma}_{\frac{1}{2}(\nu+1)})} - \dfrac{\cos(\check{\gamma}_{\frac{1}{2}(\nu+1)}z)}{\cos(\frac{1}{2}\check{\gamma}_{\frac{1}{2}(\nu+1)})} & \text{for } \nu \text{ odd} \end{cases} \tag{2.12}$$

and

$$f_\nu(z) = \sin[\nu\pi(z+\tfrac{1}{2})] \tag{2.13}$$

satisfy the boundary conditions on $z = \pm\frac{1}{2}$ for ϕ and θ, respectively. The quantities $\hat{\gamma}_{\frac{1}{2}\nu}$ and $\check{\gamma}_{\frac{1}{2}\nu+1}$ are determined from the positive roots of

$$\coth(\tfrac{1}{2}\hat{\gamma}) - \cot(\tfrac{1}{2}\hat{\gamma}) = 0, \tag{2.14}$$

$$\tanh(\tfrac{1}{2}\check{\gamma}) - \tan(\tfrac{1}{2}\check{\gamma}) = 0, \tag{2.15}$$

and are listed in Chandrasekhar (1961).

The summations in (2.10) and (2.11) are constrained by a truncation parameter N such that

$$\beta + \lambda + \nu \leqslant N. \tag{2.16}$$

All coefficients outside this range are neglected. In the numerical procedure the truncation parameter is increased until a further increase produces a negligible change in the solution. In practical terms, N is increased until a quantity such as the Nusselt number changes by less than a few percent when N is replaced by $N-2$.

After substitution of (2.10) and (2.11) into (2.7) and (2.8), multiplication by $\phi_{\gamma\kappa\mu}$ and $\theta_{\gamma\kappa\mu}$ and averaging over the fluid layer, a set of nonlinear algebraic equations for the unknowns $a_{\beta\lambda\nu}$ and $b_{\beta\lambda\nu}$ is obtained:

$$I^1_{\gamma\kappa\mu\beta\lambda\nu}a_{\beta\lambda\nu}+I^2_{\gamma\kappa\mu\beta\lambda\nu}b_{\beta\lambda\nu}+\frac{1}{P}I^3_{\gamma\kappa\mu\beta\lambda\nu\delta\rho\pi}a_{\beta\lambda\nu}a_{\delta\rho\pi}+\frac{\omega}{sP}I^4_{\gamma\kappa\mu\beta\lambda\nu}a_{\beta\lambda\nu}=0, \tag{2.17}$$

$$I^5_{\gamma\kappa\mu\beta\lambda\nu}b_{\beta\lambda\nu}+RI^6_{\gamma\kappa\mu\beta\lambda\nu}a_{\beta\lambda\nu}+I^7_{\gamma\kappa\mu\beta\lambda\nu\delta\rho\pi}a_{\beta\lambda\nu}b_{\delta\rho\pi}+\frac{\omega I^8_{\gamma\kappa\mu\beta\lambda\nu}}{s}b_{\beta\lambda\nu}=0. \tag{2.18}$$

Repeated subscripts in (2.17) and (2.18) indicate summation over λ and ν with $\lambda+\nu$ even. The calculation of the integrals $I^1,\ldots,I^8$ in these expressions is straightforward, e.g.

$$I^2_{\gamma\kappa\mu\beta\lambda\nu}=-\langle\phi_{\gamma\kappa\mu}(1+\epsilon\cos(s\omega t))\,\partial_x\theta_{\beta\lambda\nu}\rangle, \tag{2.19}$$

where the angle brackets indicate an average over the fluid layer and time. In the above expressions, $s=1$ for synchronous convection and $s=2$ for subharmonic convection.

The set of nonlinear algebraic equations (2.17) and (2.18) are solved by the Newton–Raphson iteration procedure. As the solution nears convergence, the procedure is second-order correct in the value of the coefficients, thus ensuring a solution in a minimum number of iterations, usually five or six to converge the solution to an error of 10^{-4}.

The Galerkin representation (2.10) and (2.11) can also be used to solve the linear problem of the onset of convection in which the nonlinear terms in (2.7) and (2.8) are neglected. In this case, only terms with $\lambda=1$ are taken into account in the representations (2.10) and (2.11).

2.3. *Stability of finite-amplitude solutions*

We investigate the stability of the finite-amplitude synchronous and subharmonic modes of convection to two-dimensional disturbances of different temporal character. The equations for the disturbance field $\tilde\phi,\tilde\theta$ are obtained by replacing ϕ and θ in (2.7) and (2.8) by $\phi+\tilde\phi$ and $\theta+\tilde\theta$, respectively, and subtracting from the resulting equations the equations for the finite-amplitude solution ϕ,θ:

$$\begin{aligned}\nabla^4\partial^2_{xx}\tilde\phi-(1-\epsilon\cos(s\omega t))\,\partial^2_{xx}\tilde\theta&\\ =\frac{1}{P}\Big\{&\partial^2_{xz}\phi\partial^4_{xxzz}\tilde\phi+\partial^2_{xz}\tilde\phi\partial^4_{xxzz}\phi-\partial^2_{xx}\phi\partial^4_{xzzz}\tilde\phi-\partial^2_{xx}\tilde\phi\partial^4_{xzzz}\phi\\ &+\partial^2_{xz}\phi\partial^4_{xxxx}\tilde\phi+\partial^2_{xz}\tilde\phi\partial^4_{xxxx}\phi-\partial^2_{xx}\phi\partial^4_{xxxz}\tilde\phi-\partial^2_{xx}\tilde\phi\partial^4_{xxxz}\phi+\frac{\partial}{\partial t}(\partial_{xx}\nabla^2\tilde\phi)\Big\},\end{aligned} \tag{2.20}$$

$$\nabla^2\tilde\theta-R\partial^2_{xx}\tilde\phi=\partial^2_{xz}\tilde\phi\partial_x\theta+\partial^2_{xz}\phi\partial_x\tilde\theta-\partial^2_{xx}\tilde\phi\partial_z\theta-\partial^2_{xx}\phi\partial_z\tilde\theta+\frac{\partial\tilde\theta}{\partial t}. \tag{2.21}$$

Terms that are quadratic in the disturbance amplitude in (2.20) and (2.21) have been neglected. As in the nonlinear analysis above, the parameter s assumes the value 1 for synchronous convection and 2 for subharmonic convection. For the numerical solution of (2.20) and (2.21) by the Galerkin method, we expand the functions $\tilde\phi$ and $\tilde\theta$ as

$$\begin{aligned}\tilde\phi=\sum_{\beta\lambda\nu}\{&\cos\lambda\alpha x\,(\tilde a^{11}_{\beta\lambda\nu}\cos\beta\omega t+\tilde a^{12}_{\beta\lambda\nu}\sin\beta\omega t)\\ &+\sin\lambda\alpha x\,(\tilde a^{21}_{\beta\lambda\nu}\cos\beta\omega t+\tilde a^{22}_{\beta\lambda\nu}\sin\beta\omega t)\}\,g_\nu(z)\,e^{il\alpha x+\sigma t},\end{aligned} \tag{2.22}$$

$$\begin{aligned}\tilde\theta=\sum_{\beta\lambda\nu}\{&\cos\lambda\alpha x\,(\tilde b^{11}_{\beta\lambda\nu}\cos\beta\omega t+\tilde b^{12}_{\beta\lambda\nu}\sin\omega t)\\ &+\sin\lambda\alpha x\,(\tilde b^{21}_{\beta\lambda\nu}\cos\beta\omega t+\tilde b^{22}_{\beta\lambda\nu}\sin\beta\omega t)\}\,f_\nu(z)\,e^{il\alpha x+\sigma t}.\end{aligned} \tag{2.23}$$

Substitution of (2.22) and (2.23) into (2.20) and (2.21), multiplication by $\tilde{\phi}^{11}_{\gamma\kappa\mu}$, $\tilde{\phi}^{12}_{\gamma\kappa\mu}$, $\tilde{\phi}^{21}_{\gamma\kappa\mu}$, $\tilde{\phi}^{22}_{\gamma\kappa\mu}$, and similar $\tilde{\theta}$-terms, and averaging over the fluid layer yields a set of linear algebraic equations for the unknown coefficients $\tilde{a}^{11}_{\beta\lambda\nu}$, $\tilde{a}^{12}_{\beta\lambda\nu}$, etc:

$$I^{1}_{\gamma\kappa\mu\beta\lambda\nu}\tilde{a}^{11}_{\beta\lambda\nu}+I^{2}_{\gamma\kappa\mu\beta\lambda\nu}\tilde{b}^{11}_{\beta\lambda\nu}+\frac{1}{P}\{I^{13}_{\gamma\kappa\mu\beta\lambda\nu}\tilde{a}^{11}_{\beta\lambda\nu}+I^{14}_{\gamma\kappa\mu\beta\lambda\nu}\tilde{a}^{12}_{\beta\lambda\nu}+I^{15}_{\gamma\kappa\mu\beta\lambda\nu}\tilde{a}^{21}_{\beta\lambda\nu}+I^{16}_{\gamma\kappa\mu\beta\lambda\nu}\tilde{a}^{22}_{\beta\lambda\nu}\}=\frac{\sigma}{P}I^{17}_{\gamma\kappa\mu\beta\lambda\nu}\tilde{a}^{11}_{\beta\lambda\nu} \quad (2.24)$$

and analogous expressions with leading terms $I^{21}_{\gamma\kappa\mu\beta\lambda\nu}\tilde{a}^{12}_{\beta\lambda\nu}$, $I^{31}_{\gamma\kappa\mu\beta\lambda\nu}\tilde{a}^{21}_{\beta\lambda\nu}$ and $I^{41}_{\gamma\kappa\mu\beta\lambda\nu}\tilde{a}^{22}_{\beta\lambda\nu}$. Similarly, from (2.21) we obtain

$$I^{51}_{\gamma\kappa\mu\beta\lambda\nu}\tilde{b}^{11}_{\beta\lambda\nu}+RI^{52}_{\gamma\kappa\mu\beta\lambda\nu}\tilde{a}^{11}_{\beta\lambda\nu}+I^{53}_{\gamma\kappa\mu\beta\lambda\nu}\tilde{a}^{11}_{\beta\lambda\nu}+I^{54}_{\gamma\kappa\mu\beta\lambda\nu}\tilde{a}^{12}_{\beta\lambda\nu}+I^{55}_{\gamma\kappa\mu\beta\lambda\nu}\tilde{a}^{21}_{\beta\lambda\nu}+I^{56}_{\gamma\kappa\mu\beta\lambda\nu}\tilde{a}^{22}_{\beta\lambda\nu}+I^{57}_{\gamma\kappa\mu\beta\lambda\nu}\tilde{b}^{11}_{\beta\lambda\nu}+I^{58}_{\gamma\kappa\mu\beta\lambda\nu}\tilde{b}^{12}_{\beta\lambda\nu}+I^{59}_{\gamma\kappa\mu\beta\lambda\nu}\tilde{b}^{21}_{\beta\lambda\nu}+I^{510}_{\gamma\kappa\mu\beta\lambda\nu}\tilde{b}^{22}_{\beta\lambda\nu}=\sigma I^{511}_{\gamma\kappa\mu\beta\lambda\nu}\tilde{b}^{11}_{\beta\lambda\nu} \quad (2.25)$$

and analogous expressions with leading terms $I^{61}_{\gamma\kappa\mu\beta\lambda\nu}\tilde{b}^{12}_{\beta\lambda\nu}$, $I^{71}_{\gamma\kappa\mu\beta\lambda\nu}\tilde{b}^{21}_{\beta\lambda\nu}$, and $I^{81}_{\gamma\kappa\mu\beta\lambda\nu}\tilde{b}^{22}_{\beta\lambda\nu}$. The repeated subscripts in these equations indicate summation as before. This system of linear homogeneous equations constitutes an eigenvalue problem for the eigenvalue σ. Application of ordinary numerical eigenvalue procedures requires that the indices β, λ, and ν be combined into a single subscript and coefficients $\tilde{a}^{11}$, $\tilde{a}^{12}$, etc. be combined sequentially to form a single vector.

3. Numerical results

3.1. *Onset of convection*

Before presenting the nonlinear solutions we extend the analysis of Gresho & Sani (1970) for the onset of convection to a much larger region of parameter space. Figure 1 shows the critical Rayleigh number R_c for onset of convection at Prandtl number 7 (water at room temperature) for various values of ϵ/ω^2. Figure 2 gives the corresponding values of the critical wavenumber α_c. If the external acceleration is applied by oscillating the fluid layer vertically with dimensionless frequency ω and dimensionless maximum displacement δ, then ϵ/ω^2 can alternatively be written δFr, where Fr is a Froude number defined by κ^2/gd^3. The presentation in figures 1 and 2 is thus suited to comparison with experiments carried out by oscillating fluid layers with fixed amplitude and variable frequency.

For a given ϵ/ω^2 or δFr, there are two modes of convective onset. The synchronous mode at low frequency and the subharmonic mode at high frequency; R_c increases with increasing ω for the synchronous mode while it decreases with increasing frequency for the subharmonic mode (figure 1). The crossover frequency between synchronous and subharmonic convection decreases with increasing ϵ/ω^2 or δFr; the value of R_c at the crossover point also decreases with increasing ϵ/ω^2. Synchronous convection extends to larger ω for smaller values of $\epsilon/\omega^2 = \delta Fr$ while subharmonic convection occurs at smaller ω for larger values of ϵ/ω^2. For sufficiently small ω, R_c for synchronous convection is independent of $\epsilon/\omega^2 = \delta Fr$; the increase of R_c with ω for synchronous convection occurs over a narrow range of ω near the crossover frequency to subharmonic convection. Synchronous convection occurs at smaller values of α_c than subharmonic convection (figure 2). For synchronous convection at sufficiently small ω, $\alpha_c = 3.116$ (given as 3.117 in Chandrasekhar 1961) independent of $\epsilon/\omega^2 = \delta Fr$; α_c decreases with increasing ω in a narrow range of ω near the crossover frequency to subharmonic convection. The critical wavenumber for subharmonic convection

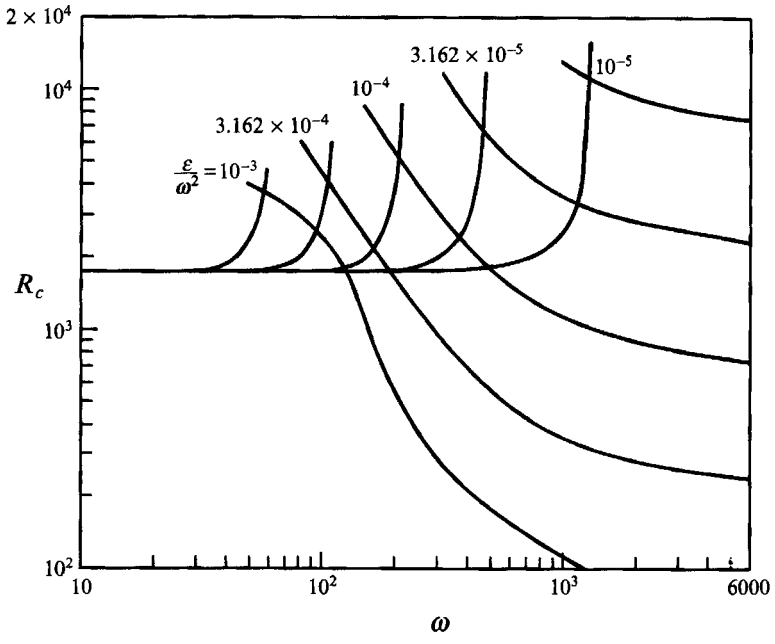

FIGURE 1. Critical Rayleigh number R_c for onset of convection in a gravitationally modulated fluid layer heated from below at $P = 7$ as a function of dimensionless frequency ω for different values of the parameter $\epsilon/\omega^2 = \delta Fr$. At low frequency convective onset is in the form of synchronous motions. At high ω convection begins subharmonically.

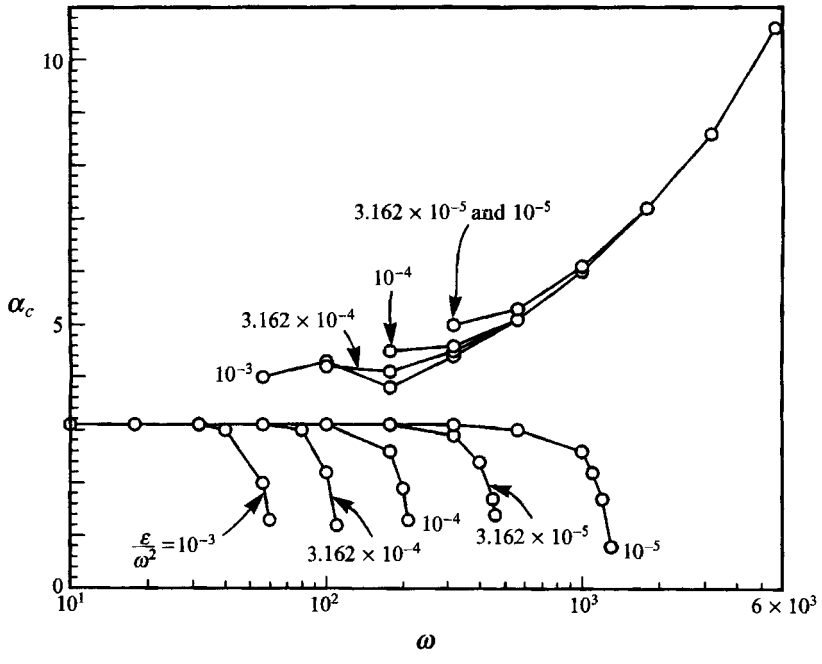

FIGURE 2. Critical wavenumber α_c at the onset of convection versus dimensionless frequency ω for $P = 7$ and for different values of $\epsilon/\omega^2 = \delta Fr$. The upper set of curves is for subharmonic motions and the lower set is for synchronous motions.

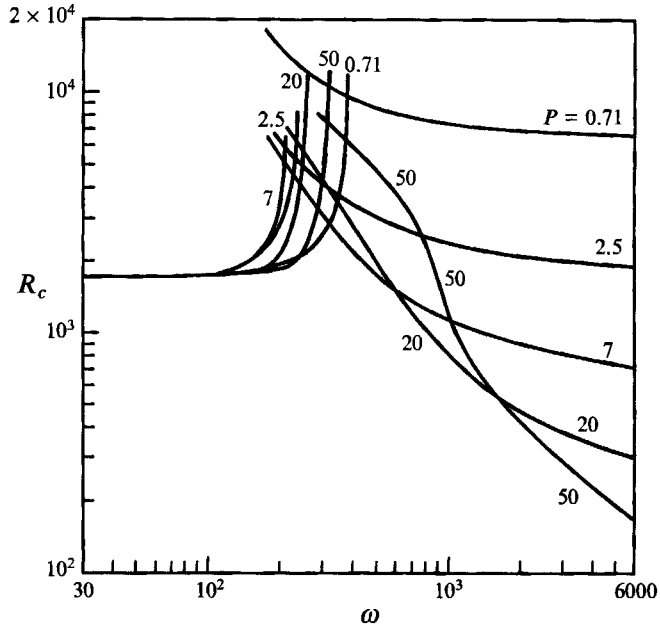

FIGURE 3. Critical Rayleigh number R_c for the onset of convection in a gravitationally modulated fluid layer heated from below with $\epsilon/\omega^2 = \delta Fr = 10^{-4}$ as a function of dimensionless frequency ω at various Prandtl numbers P. Subharmonic curves are on the right and synchronous curves are on the left. At $\omega = 0$, R_c is 1708.

generally increases with increasing ω, although α_c has a local minimum for $\epsilon/\omega^2 = \delta Fr = 10^{-3}$. The local minimum in α_c for $\epsilon/\omega^2 = 10^{-3}$ is matched by the change in curvature of R_c *vs.* ω at this value of ϵ/ω^2. For sufficiently large ω, the values of α_c for subharmonic convection tend to become independent of $\epsilon/\omega^2 = \delta Fr$. There is a discontinuous change in α_c at the transition from synchronous to subharmonic convection.

At sufficiently large ω, R_c is given by the asymptotic formula (Gresho & Sani 1970)

$$R_c \to \frac{0.4739}{P}\left(\frac{\epsilon}{\omega^2}\right)^{-1} \quad (\omega \to \infty). \tag{3.1}$$

At $P = 7$, the asymptotic regime in which (3.1) is valid lies at values of $\omega > 6000$ (figure 1). The asymptotic regime of the validity of (3.1) is computationally more accessible for smaller values of the Prandtl number as can be seen in figure 3 which illustrates the P dependence of R_c *vs.* ω for $\epsilon/\omega^2 = \delta Fr = 10^{-4}$. It is clear from the figure that increasingly large values of ω are required to reach the asymptotic state given by (3.1) as P increases. At the largest value of ω shown in figure 3, the numerically calculated R_c is within 1% of the prediction of (3.1) for $P = 0.71$; at $P = 50$, however, R_c is a factor of nearly 2 larger than the prediction of (3.1) for $\omega = 6000$.

The Prandtl number dependence of α_c *vs.* ω is illustrated in figure 4 for $\epsilon/\omega^2 = \delta Fr = 10^{-4}$. As in figure 2, it is seen that α_c increases with increasing ω at large ω, but figure 4 shows that the large-frequency limit of α_c depends on P. As $\omega \to \infty$ and for fixed ω, α_c decreases with increasing P as does R_c (figure 3); at the lower frequencies of subharmonic convective onset the dependences of α_c and R_c on P at fixed ω are non-monotonic. Similarly, the dependences of α_c and R_c on P at fixed ω for the synchronous modes of convective onset are non-monotonic (figures 3 and 4).

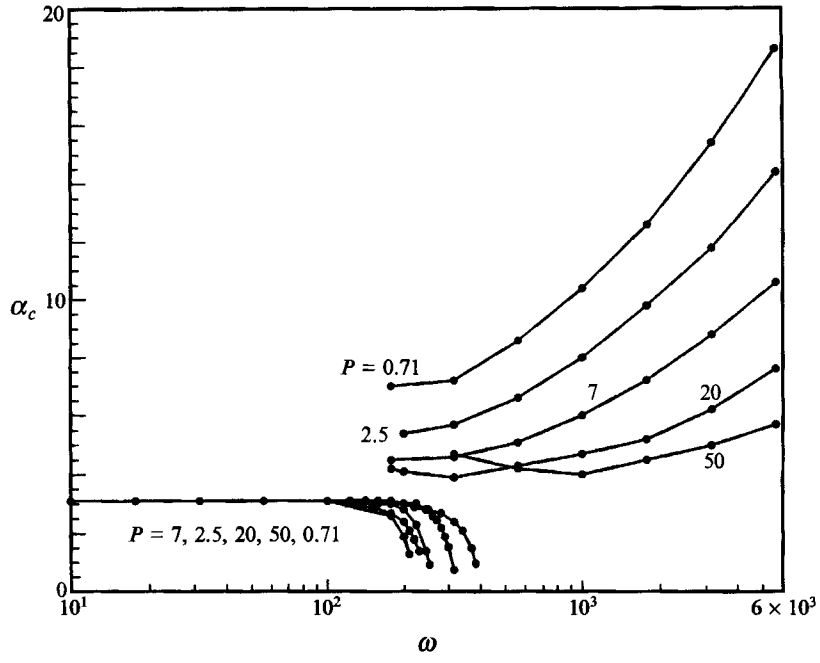

FIGURE 4. Critical wavenumber α_c versus dimensionless frequency ω for onset of convection at $\epsilon/\omega^2 = \delta Fr = 10^{-4}$ for various values of P. Upper curves are for subharmonic instability while lower curves are for synchronous instability.

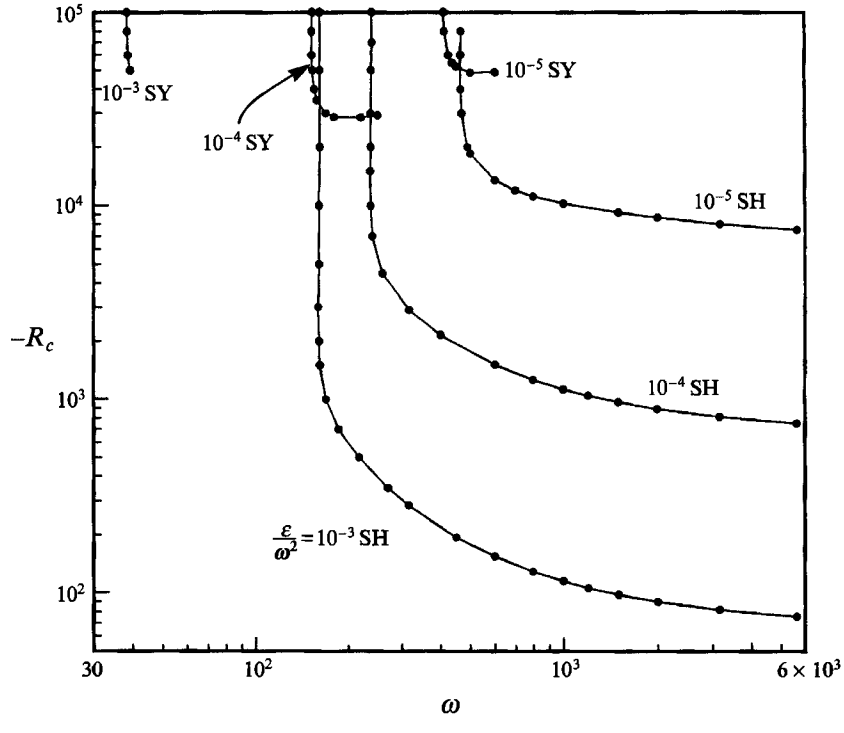

FIGURE 5. Critical Rayleigh number R_c for onset of convection in a modulated fluid layer heated from above at $P = 7$. SY denotes synchronous and SH subharmonic modes of convective onset.

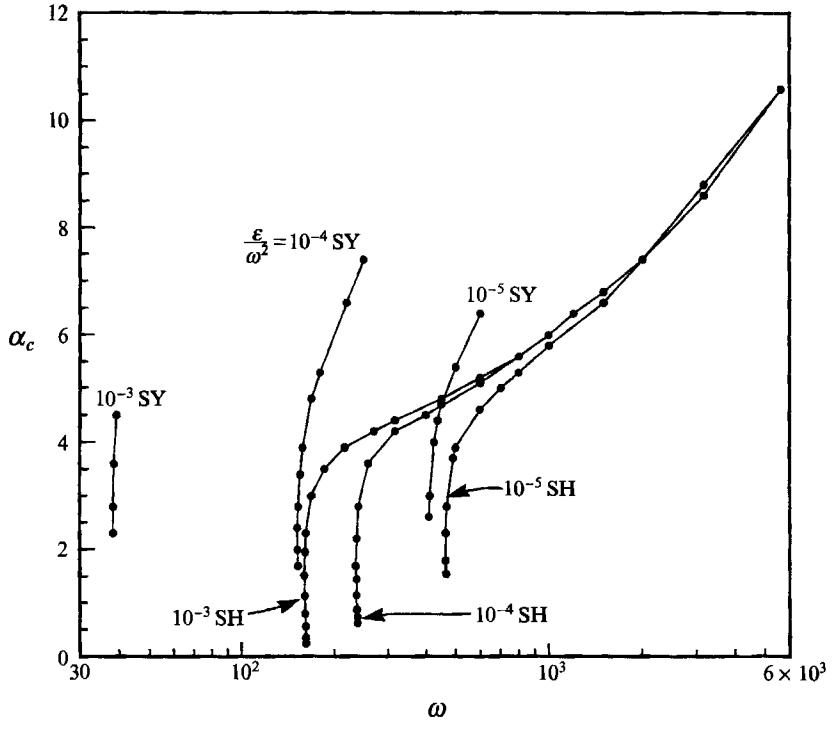

FIGURE 6. Critical wavenumber α_c versus dimensionless frequency ω for onset of convection in a gravitationally modulated fluid layer heated from above at $P = 7$. SY denotes synchronous and SH subharmonic modes of convective onset.

For sufficiently large ω convective instability is possible even for heating from above, as can be seen in figures 5 and 6 which show R_c and α_c *vs.* ω with $\epsilon/\omega^2 = \delta Fr$ as a parameter for $P = 7$. At a given value of $\epsilon/\omega^2 = \delta Fr$, convection with heating from above cannot occur until ω reaches a critical value when convection sets in as a synchronous mode. The magnitude of R_c decreases with increasing ω for the synchronous mode. Synchronous heated-from-above convection is the mode of convective onset only over a limited range of ω; with increasing ω subharmonic convection rapidly replaces synchronous convection as the preferred mode of convective onset. The magnitude of R_c decreases with increasing ω for heated-from-above subharmonic convection. The smaller the value of $\epsilon/\omega^2 = \delta Fr$ the larger ω must be for convection to occur in either the synchronous mode or the subharmonic mode. As $\omega \to \infty$, $|R_c|$ tends to a constant value that depends inversely on $\epsilon/\omega^2 = \delta Fr$, similar to the dependence in (3.1).

The critical wavenumber α_c for synchronous convective onset with heating from above increases rapidly with increasing ω in strong contrast to the behaviour of α_c *vs.* ω for bottom-heated synchronous convection (compare figures 2 and 6). Upon transition to subharmonic convective onset with heating from above and increasing ω there is a dramatic and discontinuous drop in α_c (figure 6). With further increase in ω, α_c increases for the subharmonic mode similar to the α_c *vs.* ω behaviour for subharmonic heated-from-below convection (figure 2). As ω tends to large values, α_c *vs.* ω for subharmonic heated-from-above convection tends to become independent of $\epsilon/\omega^2 = \delta Fr$. The results of figure 6 show that α_c continues to increase with increasing ω for large ω, contrary to the claim of Gresho & Sani (1970) that α_c tends to a constant

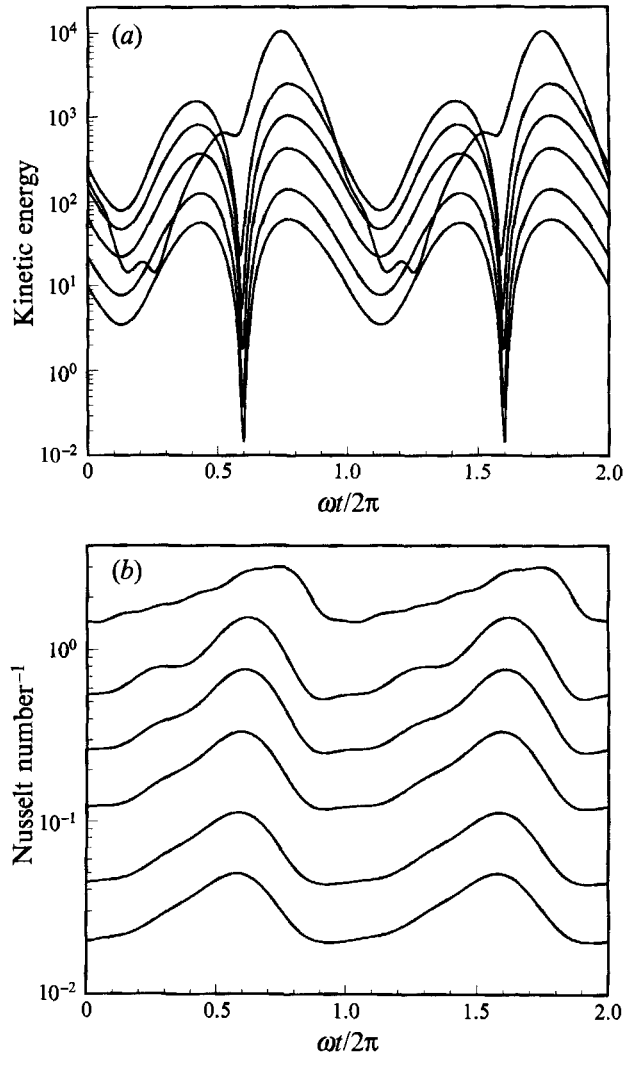

FIGURE 7. (*a*) Kinetic energy of subharmonic convection in a modulated layer at $P = 7$, $\epsilon = 3.162$, $\omega = 316.2$, $\alpha = \alpha_c = 5.0$. The Rayleigh numbers of the curves, from the bottom upwards are $R = 11700$, 12000, 13000, 15000, 20000 and 80000. (*b*) Nusselt number *vs.* $\omega t/2\pi$ for subharmonic convection at $P = 7$, $\epsilon = 3.162$, and $\omega = 316.2$. The curves correspond to different values of R, labelled as in (*a*).

as $\omega \to \infty$. The change in curvature of the α_c *vs.* ω dependence with increasing ω that occurs for large ω (figure 6) is responsible for the large-frequency asymptotic behaviour of α_c; this change in curvature occurs at values of ω larger than those considered by Gresho & Sani (1970).

3.2. *Nonlinear properties of modulated convection*

Horizontally averaged properties of both synchronous and subharmonic convection rolls exhibit the period of the applied forcing. For example, the kinetic energy of the subharmonic rolls shown in figure 7(*a*) is synchronous with the forcing, while the velocity field just reverses its sign in the second half of the subharmonic cycle. The kinetic energy decreases very quickly as the fluid becomes almost stagnant in the

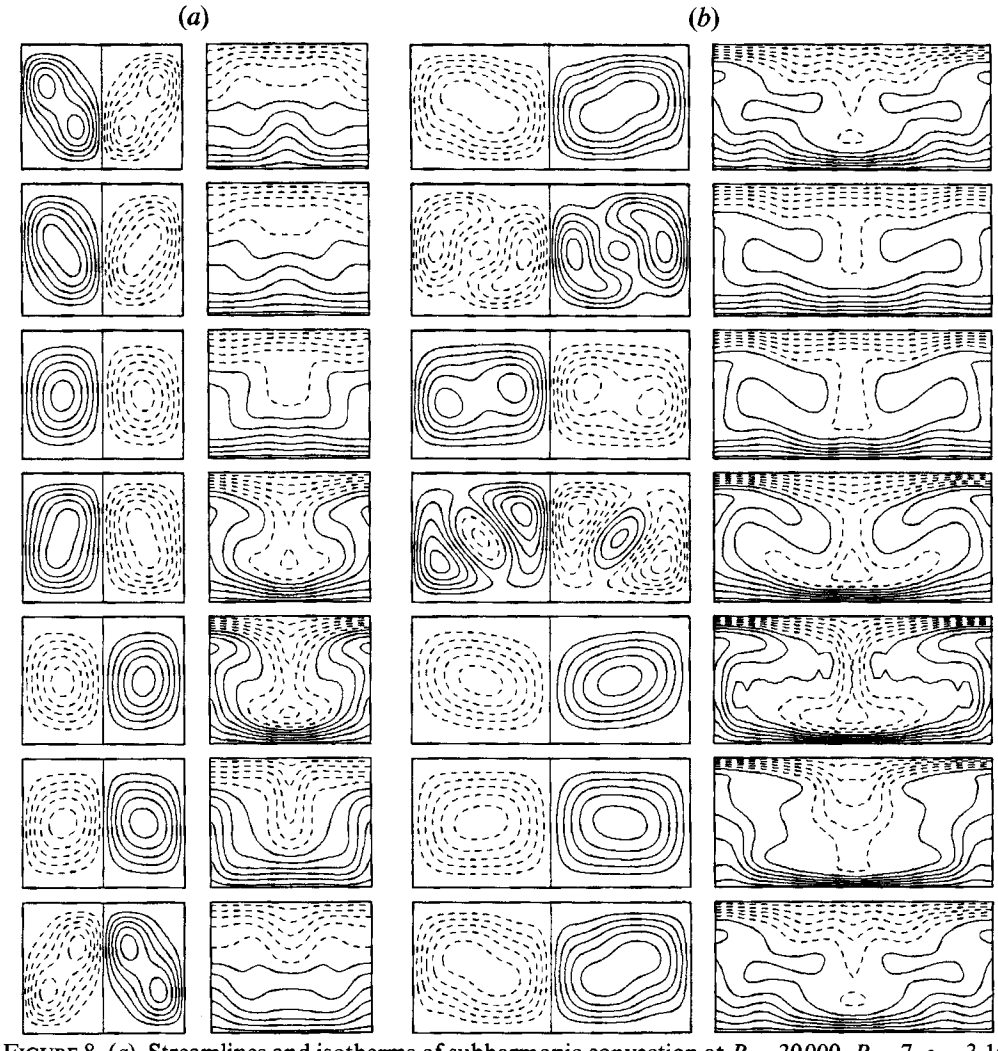

FIGURE 8. (*a*) Streamlines and isotherms of subharmonic convection at $R = 30000$, $P = 7$, $\epsilon = 3.162$, $\omega = 316.2$, $\alpha = \alpha_c = 5.0$. The plots, proceeding downward at equal steps in time, cover one modulation period. In the next modulation period the pattern is the same except for a half-wavelength shift in the x-direction. (*b*) Streamlines and isotherms of synchronous convection at $R = 40000$, $P = 7$, $\epsilon = 3.162$, $\omega = 316.2$, $\alpha = \alpha_c = 2.9$. The plots, proceeding downward at equal steps in time, cover a full modulation period. The pattern is identical in the next modulation period.

process of velocity reversal. It is evident from figure 7(*a*) that some sort of temporal transition has occurred at the highest Rayleigh number. The corresponding variation of the Nusselt number shown in figure 7(*b*) is much smoother because of the damping influence of thermal diffusion. The Nusselt number shown in the figure is the normalized horizontally averaged heat flux in the convective state and it is given by

$$Nu = 1 - \sum_{\beta\nu} \frac{\nu\pi(-1)^{\nu}}{R} [\hat{b}_{\beta 0\nu} \cos(\beta\omega t) + \check{b}_{\beta 0\nu} \sin(\beta\omega t)]. \tag{3.2}$$

The changes in the velocity field and the temperature field for the parameter values used in figure 7 are shown in figure 8(*a*). A single velocity reversal occurs during the modulation period shown in this figure. It is difficult to capture the moment of

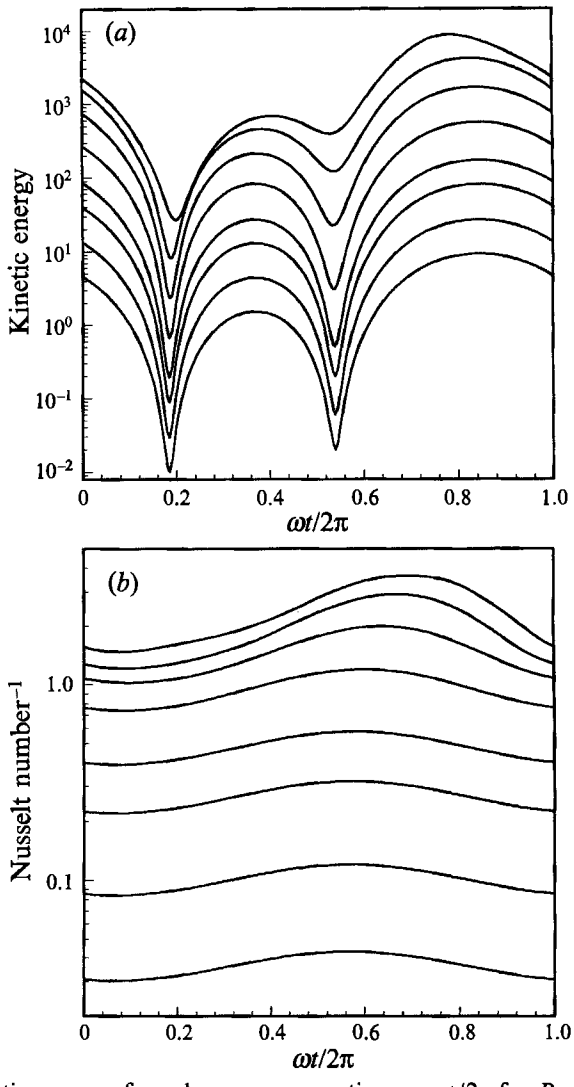

FIGURE 9. (*a*) Kinetic energy of synchronous convection *vs.* $\omega t/2\pi$ for $P = 7$, $\epsilon = 3.162$, $\omega = 316.2$, $\alpha = \alpha_c = 2.9$. R (from the bottom to top) = 2100, 2200, 2500, 3000, 5000, 10000, 20000 and 40000. (*b*) Similar to (*a*) but for the Nusselt number.

changeover in the direction of the velocity field since it occurs rather suddenly and simultaneously throughout the layer. The subharmonic motions shown in figure 8(*a*) repeat every second modulation period.

The variation in time over one modulation period for the synchronous case is shown for similar parameter values in figure 8(*b*). The synchronous motions shown in figure 8(*b*) repeat in the next modulation period. The direction of the velocity also reverses itself, twice within one period in this case, but there is no symmetry between the two states. Flow reversal in the synchronous case is related to the reversal in sign of $(1+\epsilon\cos\omega t)$ for $\epsilon > 1$. The lack of symmetry of $(1+\epsilon\cos\omega t)$ about zero accounts for the asymmetry in the synchronous states before and after velocity reversal. The two corresponding dips in the kinetic energy are clearly seen in figure 9(*a*). In figure 9(*b*), the Nusselt number shows a rather smooth dependence because the periods are short in comparison to the thermal diffusion time.

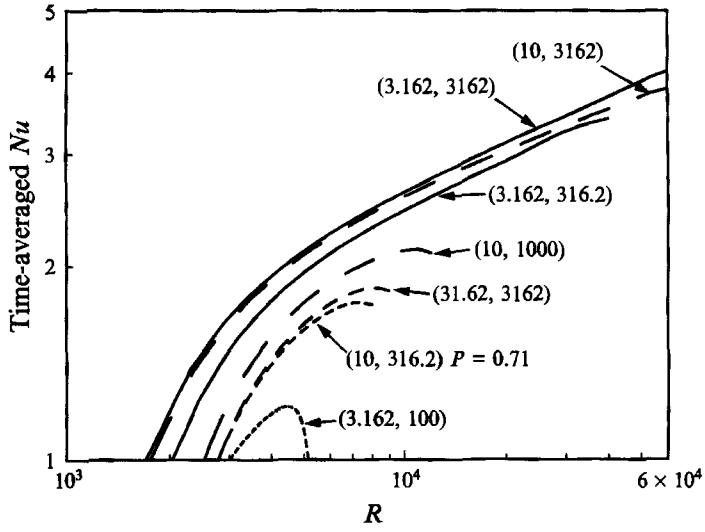

FIGURE 10. Time-averaged Nusselt number of synchronous two-dimensional convection as a function of Rayleigh number. Numbers on the curves are values of (ϵ, ω). $P = 7$ except as noted.

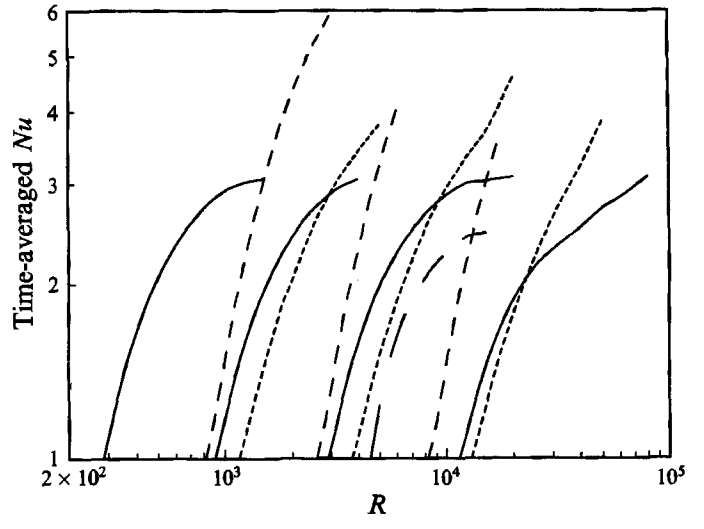

FIGURE 11. Time-averaged Nusselt number of subharmonic convection *vs.* R for $P = 7$. Long dashed line $\omega = 100$, $\epsilon = 3.162$. Solid lines (from left to right) $\omega = 316.2$, and $\epsilon = 100, 31.62, 10, 3.162$. Short dashed lines (from left to right) $\omega = 1000$, and $\epsilon = 100, 31.62, 10$. Medium dashed line (from left to right) $\omega = 3162$, and $\epsilon = 1000, 316.2, 100$.

Figure 10 shows the time-averaged Nusselt number of synchronous two-dimensional convection as a function of Rayleigh number for various values of ω and ϵ. For small ϵ and large ω the results differ little from unmodulated convection. As ω is decreased from a large value at fixed ϵ, the Nusselt number decreases, mainly due to an increase in the critical Rayleigh number for onset of convection. For large values of ϵ the Nusselt number first increases with increasing Rayleigh number, but then begins to decrease as is evident from the lowest four curves in figure 10. This behaviour is most clear in the lowest curve for $\epsilon = 3.162$ and $\omega = 100$, for which convection disappears completely at a Rayleigh number of about 5×10^3.

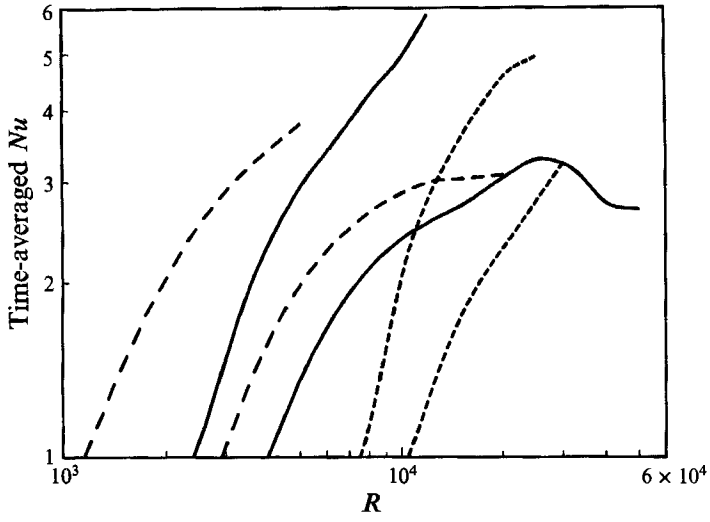

FIGURE 12. Time-averaged Nusselt number of subharmonic convection versus Rayleigh number for different Prandtl numbers. Long dashed lines correspond to $P = 7$, solid lines to $P = 2.5$, and short dashed lines to $P = 0.71$. The left (right) curve of each pair corresponds to $\epsilon = 100(10)$ $\omega = 1000$ (316.2).

Time-averaged Nusselt numbers of subharmonic convection for $P = 7$ are shown in figure 11. The curves are similar for different values of ϵ at a fixed value of the frequency. All curves exhibit a steep initial increase of the Nusselt number with the Rayleigh number. For the smallest value of ω shown, the Nusselt number then quickly bends over and levels off at about 2.5. The bending over takes place at a higher Nusselt number of about 3 for the next value of $\omega = 316.2$. For $\omega = 1000$ this bending over is much less pronounced and, at least for two of the curves, is followed by an inflexion point and a further rapid increase in Nusselt number versus Rayleigh number. At $\omega = 3162$ the bending over is no longer noticeable and it is possible that again an inflexion point will occur. It was not possible, however, to obtain reliable numerical results for Nusselt numbers higher than those shown in figure 11. The truncation parameter necessary for calculations of the results shown in figure 11 (and figure 12 as well) typically increases with increasing Nusselt number, and all curves were calculated with the highest possible truncation parameter, $N = 16$. At $N = 16$ the rank of the coefficient matrix is 1368 and a typical solution of six iterations requires about 10 hours of computer time on a Microvax III (3500).

The influence of Prandtl number P on the heat transport of subharmonic convection can be inferred from figure 12. The variation of the heat transport with P is not as smooth as in the case of convection without modulation, even if one takes into account the dependence of the onset of convection on the Prandtl number. For example, the second solid curve in figure 12 exhibits a surprising bump which could indicate a resonance phenomenon near the Rayleigh number of about 2.5×10^4. It certainly does not represent a numerical effect since the heat transports computed with the truncations $N = 12$, 14, and 16 yield coincident results within the thickness of the curves of figure 12. The resonance could be related to the BE3-blob instability mentioned by Bolton, Busse & Clever (1986), which corresponds to three hot blobs circulating around the convection roll. However, a detailed analysis establishing such a connection has not been made.

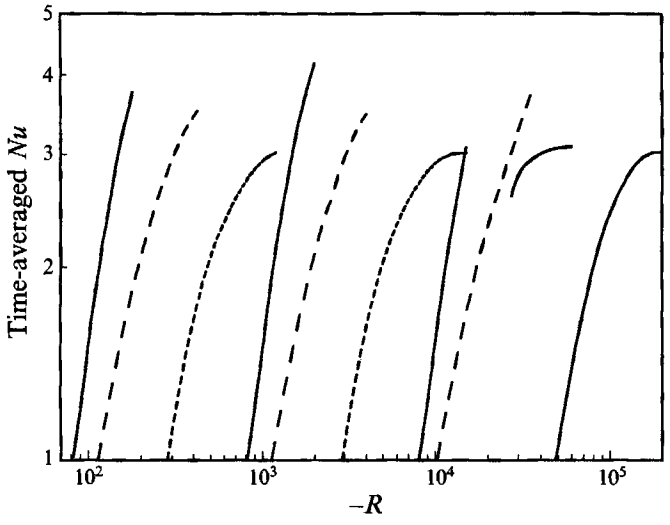

FIGURE 13. Time-averaged Nu *vs.* $-R$ for convection in a modulated fluid layer heated from above. The three leftmost solid lines correspond to (from left to right) subharmonic convection with $\omega = 3162$, and $\epsilon = 10^4$, 10^3, 10^2. Medium dashed lines (from left to right) are for $\omega = 1000$, and $\epsilon = 10^3$, 10^2, 10. Short dashed lines (from left to right) are for $\omega = 316.2$ and $\epsilon = 10^2$, 10. The two rightmost solid curves correspond to synchronous convection and $\epsilon = 4.84$, $\omega = 220$ (left) and $\epsilon = 2.5$, $\omega = 500$ (right). Note the emergence of subcritical synchronous convection for $\epsilon = 4.84$, $\omega = 220$.

Time-averaged Nusselt numbers for convection in a modulated fluid layer heated from above are shown in figure 13. The curves for subharmonic convection at large ϵ and ω are quite similar to those presented in figure 11. Indeed, when the imposed oscillating gravitational field is large compared to gravity, the cases of heating from above and below become identical. This is already apparent in the results for the onset of subharmonic convection at large ϵ and ω as shown in figures 1 and 5. Synchronous convection in the heated-from-above case, however, has no analogous counterpart in the heated-from-below case. For heating from below, synchronous convection represents a mere quantitative modification of unmodulated convection unless $\delta Fr = \epsilon\omega^{-2}$ becomes rather large. It is interesting to note the emergence of subcritical synchronous convection for $\epsilon = 4.84$ and $\omega = 220$, which corresponds to $\delta Fr = 10^{-4}$. Attempts to extend these results to lower values of δFr or to lower values of ω at constant $\delta \mathrm{Fr} = 10^{-4}$ have not been successful. The numerical solutions for these other parameter values did not converge.

Typical streamline patterns and isotherms for subharmonic convection in a modulated layer heated from above are shown in figure 14(*a*). As can be seen by comparing with figure 8, the streamlines and isotherms resemble those in the heated-from-below case. Streamlines and isotherms of synchronous convection in a modulated fluid layer heated from above are shown in figure 14(*b*). The flow reversal that occurs during a short part of the cycle also takes place in the heated-from-below case for larger values of ϵ and ω. The nearly horizontal alignment of the isotherms for a large portion of the cycle indicates the low amplitude of the convective motions. A sudden eruption of the thermal plume which provides most of the heat transport occurs from this nearly quiescent state.

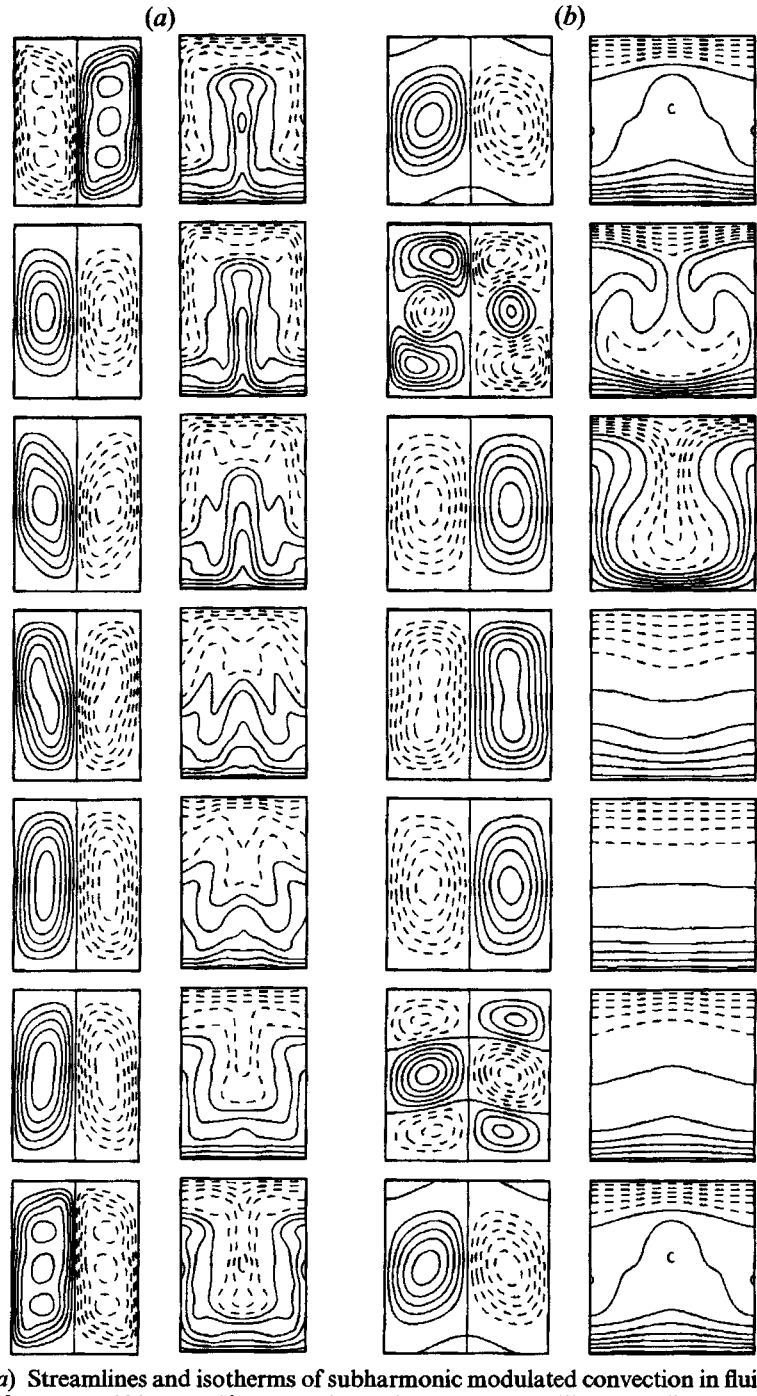

FIGURE 14. (*a*) Streamlines and isotherms of subharmonic modulated convection in fluid layer heated from above for $R = -180$, $\epsilon = 10^4$, $\omega = 3162$, and $\alpha = \alpha_c = 8.6$. (*b*) Streamlines and isotherms of synchronous modulated convection in a layer heated from above for $Ra = -60000$, $\epsilon = 4.84$, $\omega = 220$, and $\alpha = \alpha_c = 6.6$.

3.3. *Stability of synchronous convection to subharmonic disturbances*

Using the procedure outlined in §2.3, we have investigated the stability of synchronous two-dimensional oscillatory convection to subharmonic disturbances. In this procedure, only disturbances with the same horizontal structure and the same time periodicity as the nonlinear solution are considered. The stability analysis is thus limited to disturbances with the same basic wavenumber or multiples thereof as the synchronous convection. Although this stability analysis is incomplete and does not consider the transition to a quasi-periodic state, it is useful for comparing the relative stability of synchronous and subharmonic convection. The results show a transition from synchronous to subharmonic convection at a Rayleigh number somewhat higher than the extension of the curves for subharmonic onset into the synchronous regime in figures 1 and 3. The fact that the presence of finite-amplitude synchronous convection causes only a small delay in the onset of subharmonic convection indicates a strong preference for the latter mode of convection. No transition of the opposite kind, from subharmonic to synchronous convection, has been found for increasing Rayleigh number.

4. Concluding remarks

Our attempt at a reasonably systematic investigation of nonlinear convection in a layer subject to an oscillating gravity force has revealed a number of interesting features which may stimulate further experimental research on this problem. A main result is the possibility of severe reductions of the convective heat transport for certain values of the parameters as indicated in figure 10. For other parameter values the heat transport may be enhanced in comparison with the unmodulated case through the effects of resonance. A question that could not be answered by the theoretical analysis of this paper is the stability of the two-dimensional solutions with respect to three-dimensional disturbances. Obviously, as is well known from the case of steady gravity, convection rolls are likely to become unstable through various mechanisms as the Rayleigh number is increased beyond the critical value. But from the available information in the literature there is little evidence that the stability of rolls is much reduced by the presence of an oscillatory component of gravity. The competition between rolls and hexagons that is observed in the analogous experiments with a time-modulated boundary temperature (Meyer *et al.* 1988; Meyer, Cannell & Ahlers 1992) is clearly caused by the asymmetry introduced by the oscillatory boundary condition.

Even in the case of the layer heated from above, rolls are likely to be the preferred form of convection. The close analogy of this problem with the Faraday (1831) problem of surface waves induced by an oscillating gravity field in a horizontal fluid layer could suggest a preference for the same kind of pattern. While square patterns are typically observed in the latter problem (Ezerskii, Rabinovich & Korotin 1985; Douady & Fauve 1988; Ramshankar & Gollub 1991, and earlier papers referenced therein), preliminary computations for the symmetric case treated here have indicated the stability of rolls with respect to square-pattern disturbances.

The research reported in this paper was supported by the National Science Foundation under Grant CTS8915442. The authors thank N. Anderson for her assistance in the preparation of this manuscript.

REFERENCES

AHLERS, G., HOHENBERG, P. C. & LÜCKE, M. 1985*a* Thermal convection under external modulation of the driving force. I. The Lorenz model. *Phys. Rev.* A **32**, 3493–3518.

AHLERS, G., HOHENBERG, P. C. & LÜCKE, M. 1985*b* Thermal convection under external modulation of the driving force. I. Experiments. *Phys. Rev.* A **32**, 3519–3533.

BIRINGEN, S. & PELTIER, L. J. 1990 Numerical simulation of 3-D Bénard convection with gravitational modulation. *Phys. Fluids* A **2**, 754–764.

BOLTON, E. W., BUSSE, F. H. & CLEVER, R. M. 1986 Oscillatory instabilities of convection rolls at intermediate Prandtl numbers. *J. Fluid Mech.* **164** 469–485.

BURDE, G. I. 1970 Numerical study of the onset of convection in a modulated field of external forces (in Russian). *Izv. Akad. Nauk SSSR, Mekh. Zhid. Gazov*, **2**, 196.

CHANDRASEKHAR, S. 1961 *Hydrodynamic and Hydromagnetic Stability*. Clarendon.

DAVIS, S. H. 1976 The stability of time-periodic flows. *Ann. Rev. Fluid Mech* **8**, 57–74.

DONNELLY, R. J. 1990 Externally modulated hydrodynamic systems. In *Nonlinear Evolution of Spatio-Temporal Structures in Dissipative Continuous Systems* (ed. F. H. Busse & L. Kramer), pp. 31–43. Plenum.

DOUADY, S. & FAUVE, S. 1988 Pattern selection in Faraday instability. *Europhys. Lett.* **6**, 221–226.

EZERSKII, A. B., RABINOVICH, M. I. & KOROTIN, P. I. 1985 Random self-modulation of two-dimensional structures on a liquid surface during parametric-excitation. *JETP Lett.* **41**, 157–160.

FARADAY, M. 1831 Other forms and states assumed by fluids in contact with vibrating elastic surfaces. *Phil. Trans. R. Soc. Lond.* **121**, 319–340.

FINUCANE, R. G. & KELLY, R. E. 1976 Onset of instability in a fluid layer heated sinusoidally from below. *Intl J. Heat Mass Transfer* **19**, 71–85.

GERSHUNI, G. Z. & ZHUKOVITSKII, E. M. 1976 *Convective Stability of Incompressible Fluids* (translated from the Russian by D. Louvish). Jerusalem: Keter Publications.

GRESHO, P. M. & SANI, R. L. 1970 The effects of gravity modulation on the stability of a heated fluid layer. *J. Fluid Mech.* **40**, 783–806.

HOHENBERG, P. C. & SWIFT, J. B. 1987 Hexagons & rolls in periodically modulated Rayleigh–Bénard convection. *Phys. Rev.* A **35**, 3855–3873.

MEYER, C. W., AHLERS, G., CANNELL, D. S., HOHENBERG, P. C. & SWIFT, J. B. 1988 Pattern competition in temporally modulated Rayleigh–Bénard convection. *Phys. Rev. Lett.* **61**, 947–950.

MEYER, C. W., CANNELL, D. S. & AHLERS, G. 1992 Hexagonal and roll flow patterns in temporally modulated Rayleigh–Bénard convection. *Phys. Rev.* A **45**, 8583–8604.

NIEMELA, J. J. & DONNELLY, R. J. 1987 External modulation of Rayleigh–Bénard convection. *Phys. Rev. Lett.* **59**, 2431–2434.

RAMSHANKAR, R. & GOLLUB, J. P. 1991 Transport by capillary waves 2. Scalar dispersion and structure of the concentration field. *Phys. Fluids* A **3**, 1344–1350.

ROPPO, M. N., DAVIS, S. H. & ROSENBLAT, S. 1984 Bénard convection with time-periodic heating. *Phys. Fluids* **27**, 796–803.

ROSENBLAT, S. & HERBERT, D. M. 1970 Low-frequency modulation of thermal instability. *J. Fluid Mech.* **43**, 385–398.

ROSENBLAT, S. & TANAKA, G. A. 1971 Modulation of thermal convection instability. *Phys. Fluids* **14**, 1319–1322.

VENEZIAN, G. J. 1969 Effect of modulation on the onset of thermal convection. *J. Fluid Mech.* **35**, 243–254.